32nd International Cosmic Ray Conference, Beijing 2011

Galactic Cosmic Rays: Measurements, Models and Methods

Scott P. Wakely[1)]

Enrico Fermi Institute & Department of Physics, University of Chicago, Chicago, IL 60637 USA

Abstract: This paper is based on a rapporteur talk delivered at the 32nd International Cosmic Ray Conference, held in Beijing China, in August, 2011. The object of the talk and paper is to provide a summary of the work presented in the OG1 sessions of that conference. The OG1 sessions are broadly focussed on Galactic cosmic-ray origins and cover topics in direct measurements (OG1.1), cosmic-ray sources and composition (OG1.2), propagation (OG1.3), acceleration (OG1.4) and new experiments and instrumentation (OG1.5).

Key words: Cosmic Rays; Direct Measurements; Composition; Energy Spectra

1 Introduction

In this paper, I attempt to summarize the work presented in the OG1 (Origin and Galactic Phenomena) session of the 32nd International Cosmic Ray Conference, held in August of 2011 in Beijing China. The number of papers presented in this session exceeded 100 and covered a broad range of topics, from direct measurements of cosmic rays, to studies of Galactic magnetic fields, to computer simulations of supernova dynamics. Rather than attempt to inventory each and every submission, I have tried to restrict myself to highlighting a set of results which, in my mind, capture something of the state of the art in our field. This is clearly a subjective process and I apologize if I omit something. It is probably worth noting at the start that I inevitably bring an experimentalist's bias to the topics I have chosen.

My overall impression is that, as we approach the 100th anniversary of the discovery of cosmic rays, the field is as exciting and vibrant as ever. New instruments and techniques are providing a wealth of high-precision data which, if they prove accurate, will challenge our simplest models of cosmic-ray origins and propagation. While in some cases, the presented data have been shown or hinted at in previous years, this conference was notable for the quality and cumulative impact of so many interesting results. In addition, theoretical and computational studies have kept pace with the observational developments, putting us in an excellent position test these data against our models.

This paper is organized roughly according to observational targets and I have tried to integrate discussions of theoretical works in with the topics they address. In Section 2 I will discuss light nuclei, followed by heavy nuclei in Section 3 and electrons in Section 4. Studies of cosmic-ray anti-particles are covered in Section 5. A discussion of new instrumentation is covered in 6 and I conclude in Section 7.

A note: I have primarily taken figures directly from original papers and talks, as presented at the conference. Hence, when looking at, for instance, particle spectra, attention should be paid to the units of the abscissa, which vary from total particle energy, to energy per nucleon, to rigidity. This can complicate comparisons between experiments, as conversion between the binned quantities is not always trivial.

2 Light ($Z < 3$) Nuclei

As the most abundant of the cosmic-ray species, light nuclei — hydrogen/protons and helium — of-

1) E-mail: wakely@uchicago.edu

DOI: 10.7529/ICRC2011/V12/R02

fer experimenters the best opportunity to make very high-statistics measurements of the primary cosmic-ray flux. These measurements, in turn, provide an excellent opportunity to test our models about the nature and origin of the cosmic rays. At this conference, we heard about new high-statistics measurements of light nuclei from the PAMELA collaboration, and received updated information on similar, higher-energy, measurements from the CREAM group.

The PAMELA (Payload for Antimatter-Matter Exploration and Light-nuclei Astrophysics) team presented newly-published results [1] on the spectra of cosmic-ray hydrogen and helium nuclei [2, 3]. These results are interesting in that they show several features which do not fit into the most simple "standard model" of cosmic-ray acceleration and propagation. In particular, they show that 1) the spectra of helium and hydrogen ions have different slopes, and 2) that these spectra deviate from a pure power-law form. While similar results to these have been shown recently at somewhat higher energies (see below), the PAMELA results are unique for the statistical power of the measurements.

PAMELA is a space-based magnetic spectrometer featuring a 0.43 T permanent magnet instrumented with 6 internal planes of silicon-strip tracking detectors. The instrument features an overall acceptance of 21.5 cm^{2}sr, and a maximum detectable rigidity (MDR) exceeding 1 TV. In addition to the spectrometer, which can be used for charge separation, the instrument has a time-of-flight system, a neutron detector, and a 16.3 radiation length (r.l.) silicon/tungsten sampling calorimeter.

Figure 1 shows the cosmic-ray hydrogen and helium flux, plotted vs. particle rigidity, R. The ordinate has been weighted by a factor of $R^{2.7}$. This plot includes data collected by the PAMELA instrument between 2006 and 2008. The systematic uncertainty in the flux is indicated by the pink-outlined region. This is dominated at high rigidity by uncertainty related to the imperfect knowledge of the spectrometer tracker alignment. The green lines above 30 GV are fits using a single power law functional form. The results of the fits are $\gamma_p = 2.820 \pm 0.003(\text{stat}) \pm 0.005(\text{sys})$ and $\gamma_{\text{He}} = 2.732 \pm 0.005(\text{stat})^{+0.008}_{-0.003}(\text{sys})$.

Also shown on the plot are three calculations — one which uses the standard GALPROP [4] simulation code and two which are variants of a 3-component model by Zatsepein and Sokolskaya (ZS, [5]). The 3-component model is based on the two-component model of Bierman [6], but adds a contribution of lower-energy cosmic rays produced in novae.

In the plot, the original ZS model is shown in blue, and in red is shown a version where the 3 source contributions have adjusted to fit the PAMELA data. Of particular note is the upturn in the spectra of both elements beyond ~ 100 GV.

To reduce certain systematic errors (associated with, for instance, the tracker alignment) a ratio can be constructed from the flux data. This is shown in Figure 2, along with a power-law fit (green line) above rigidities of ~ 5 GV. The standard picture of cosmic-ray acceleration and propagation predicts this line to be flat (i.e., $\gamma = 0$ — see dotted red line), whereas the

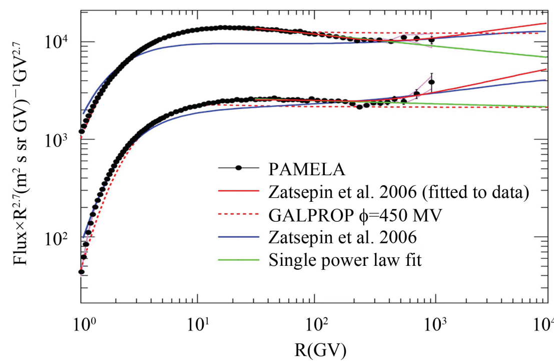

Fig. 1. Proton and helium rigidity spectra (weighted by $R^{2.7}$), as measured by the PAMELA instrument. The pink bounded region denotes the overall systematic flux uncertainty. Shown in green is a simple power-law fit above 30 GV. The dashed red line is a calculation using the GALPROP code. The blue line and red lines are predictions using the 3-component model of Zatsepein and Sokolskaya. See text for details.

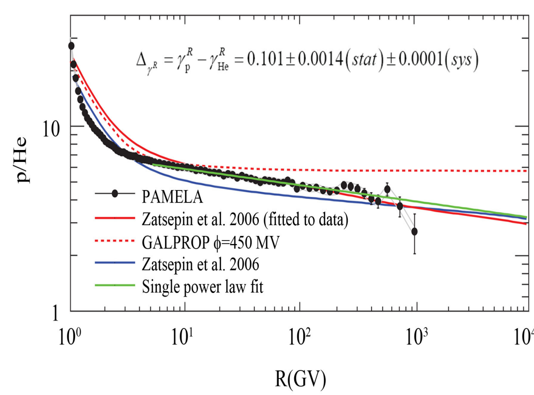

Fig. 2. Proton/Helium ratio vs rigidity, as measured by the PAMELA instrument. The systematic uncertainty (which now excludes the tracker uncertainty) is indicated by the grey bounded region. The model lines are as in Figure 1.

fit shows a statistically strong deviation from this prediction, with $\Delta\gamma = -0.101 \pm 0.0014(\text{stat}) \pm 0.0001(\text{sys})$.

Results on the p/He ratio were also presented by the CREAM collaboration [7]. CREAM (Cosmic-Ray Energetics And Mass), is a balloon-borne instrument designed for direct measurements of cosmic-ray elemental spectra to high energy. Data from the CREAM-I flight were presented. This payload consisted of a scintillator-based charge detector, a transition radiation detector, a Cerenkov detector, a silicon-based charge detector, and a tungsten/scintillating-fiber calorimeter. The geometric factor of the instrument for H and He particles (the detection of which require an interaction in the calorimeter) is ~ 0.43 m^{2}sr.

The recently-published [8] results, follow up on work previously introduced in [9], and cover the energy range $\sim 2.5 - 250$ TeV/particle. Figure 3 shows the weighted energy spectra (NB: energy per particle) for protons and helium (open circles-protons, filled circles-helium), along with the results of power-law fits. The best-fit indices ($\gamma_p = 2.66 \pm 0.02$(stat) and $\gamma_{\text{He}} = 2.58 \pm 0.02$(stat)) suggest a continuation of the behavior seen at lower rigidity by PAMELA, though the difference in the spectral indices has a lower statistical significance ($\sim 3\sigma$).

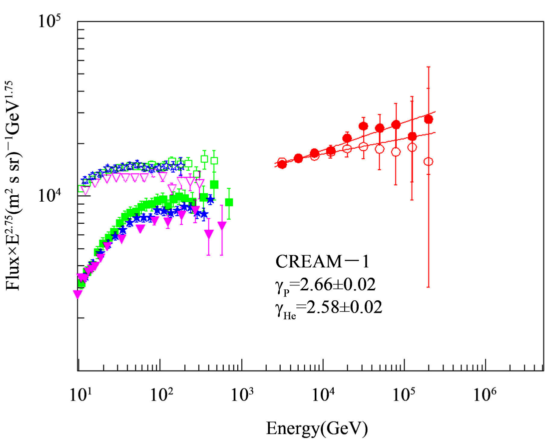

Fig. 3. Differential fluxes of cosmic-ray protons (open circles) and helium (filled circles), as measured by the CREAM-I instrument. Also shown are results from several other instruments, with open symbols representing protons and filled symbols representing helium: AMS (stars), BESS (squares), CAPRICE (inverted triangles). The results of a power-law fit to the CREAM-I H and He spectra are shown, with statistical errors.

In addition to the flight I data, the CREAM group presented results from the CREAM-III flight of 2007[7, 19]. The payload for this flight was similar to the CREAM-I payload, but doubles the number of silicon charge detectors and replaces the transition radiation detector with an aerogel ring-imaging Cerenkov detector (CHERCAM). The preliminary results from the 29-day flight appear consistent with the data from the first flight, and extend somewhat lower in energy.

As shown in Figure 4, placing the above p/He data, along with those of ATIC-2, onto a single plot reveals an interesting and conspicuous trend to lower p/He ratios with higher rigidity. In the absence of some as-yet unidentified systematic effect(s), this plot makes a powerful statement in the long-standing controversy over whether there is, in fact, a difference in the slope of the H and He spectra — a controversy which has been fueled by poor statistics and systematic disagreements between experiments. Results supporting a difference have been presented at high energy in the past by the JACEE group [10], the SOKOL group [11], and more recently, by the ATIC Collaboration [12–14]. No difference was reported by the RUNJOB group [15]. At lower energy, data from AMS-01, another space-based magnet spectrometer instrument, appear to be marginally inconsistent with no difference [16].

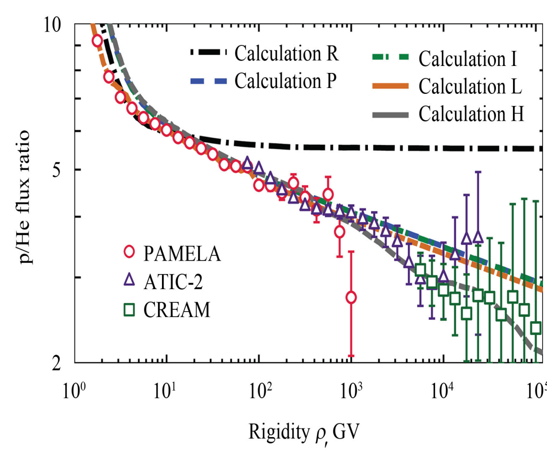

Fig. 4. Compilation of p/He measurements, plotted versus rigidity. Included on the plot are the results of several calculations, as discussed below. Plot taken from [17].

A second interesting feature of the hydrogen and helium data was highlighted by the PAMELA team. This feature involves the intrinsic shape of the proton and helium spectra[3]. It can be seen in Figure 1 that for both of these elements, there are slight deviations at high rigidity from the pure power-law fits shown with the green lines. A zoomed view of the high-R region is shown in Figure 5, where the flux has been weighted by a factor of $R^{2.7}$ to accentuate small changes. An apparent hardening in the spectral slope can be seen in both elements at $R \sim 240$ GV.

According to the PAMELA team, the hypothesis of a single power-law fit above 30GV is ruled out in these data at the 95% or greater confidence level (using the Fisher and Student-T tests)*. As an alternative to the single power law, in this figure each particle species is fit with two separate power laws. One is in the rigidity range of $30- \sim 240$GV and another is in the range R$> \sim 240$GV. The results quoted for these regions are: $\gamma_{80-232\,\mathrm{GV};p} = 2.85 \pm 0.015$, $\gamma_{>232\,\mathrm{GV};p} = 2.67 \pm 0.03$, and $\gamma_{80-240\,\mathrm{GV;He}} = 2.77 \pm 0.01$, $\gamma_{>240\,\mathrm{GV;He}} = 2.48 \pm 0.06$. The position of the spectral break is identified as 232^{+35}_{-30} GV for protons and 242^{+27}_{-31} GV for helium.

The existence of a spectral break is, again, not predicted in the standard model of cosmic-ray physics. If real, such a break likely implies some new source or new propagation physics, though as pointed out in [1], heliospheric effects, i.e., solar modulation, may play some role in explaining or partially explaining, the deviations. Of particular interest here is the fact that, as noted in [17], the p/He ratio is — within errors — continuous throughout the apparent breakpoint region, which has implications for its possible origin.

In addition to the apparent spectral break at ~ 240 GV, the PAMELA team also discussed a possible "dip" in the spectrum just prior to the break. Again, referring to Figure 5, it may be imagined that there is some spectral curvature in the transition region between the low-rigidity power law and the high-rigidity power law. That is, the extrapolation of the low-rigidity power law overshoots the data at the breakpoint, forming the dip. This is more obvious in the helium spectrum than in the hydrogen spectrum, though in both cases it seems as though the feature results from the positioning of only one or two data points.

Evidence for spectral hardening was also claimed by the CREAM group [7]. Following [9], and working with data gathered during the first flight of the instrument, they too discuss apparent breaks in the hydrogen and helium spectra. However, because the energy threshold for the calorimeter on this instrument is ~ 2.5 TeV/particle for light nuclei and the TRD is only sensitive to heavier nuclei, $Z > 3$, the CREAM measurements of H and He begin at a relatively high rigidity. Thus, unlike with the PAMELA data, which span the entire rigidity range of the claimed breakpoints, the H and He breaks here have been inferred by comparing CREAM data at higher energy to AMS data at lower energy [18].

On the other hand, CREAM measurements of heavy nuclei extend as low as $\sim$ 20 GeV/nuc, as shown in Figure 6. Here, the data (NB: units are energy/nucleon) are from the first two CREAM flights and the fluxes of the elements (C, O, Ne, Mg, Si, Fe) have been normalized to match carbon. A broken power-law fit is presented over the energy range

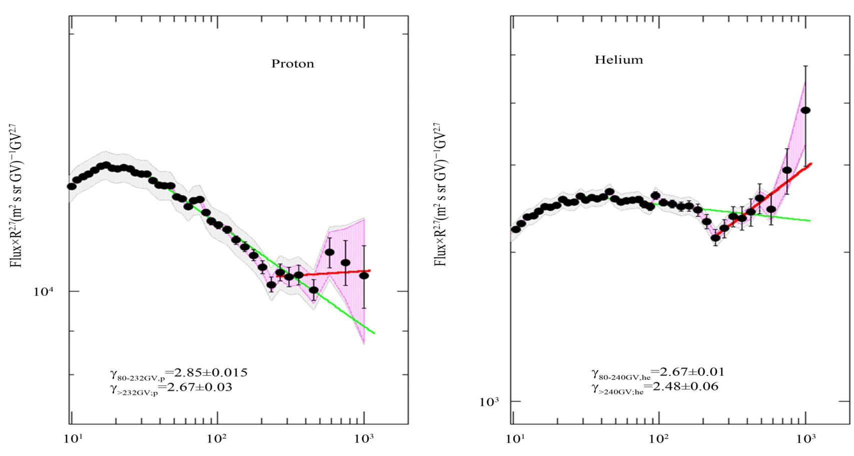

Fig. 5. Weighted fluxes of cosmic-ray protons and helium vs rigidity, as measured by the PAMELA instrument. The shaded regions denote the overall systematic uncertainty (grey) and the uncertainty derived solely from imperfect knowledge of the tracker alignment (pink). Also indicated on the plot are the spectral fits for the rigidity range $30- \sim 240$ GV (green) and $R > \sim 240$GV (red). The indices of the fits are shown at the bottom of the plot, with statistical and systematic errors added in quadrature.

*Several other statistical tests, resulting in rejections of up to 99.9% CL, are discussed in [1].

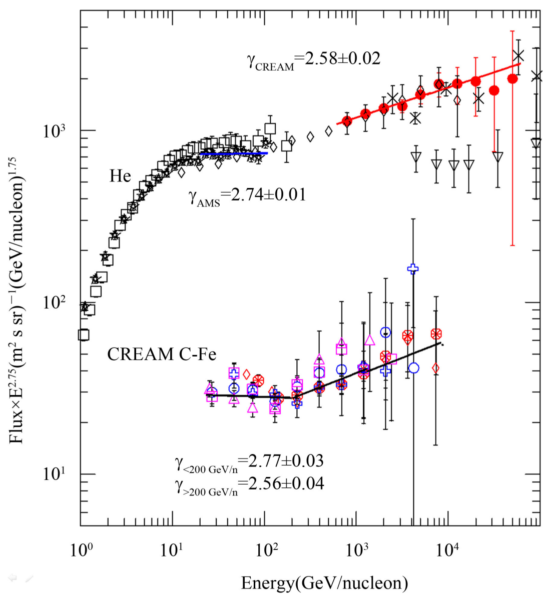

Fig. 6. Measurements of differential fluxes for several species of cosmic-ray nuclei. At the top is shown helium spectra from a number of detectors: BESS (open squares), AMS (open stars), ATIC-2 (open diamonds), JACEE ("X"), and RUNJOB (inverted open triangles). A fit to the AMS data between 20 GeV/nuc and 100 GeV/nuc is shown with the blue line. A fit to the CREAM-I data above ~ 600 GeV/nuc is shown in red. Below this is shown CREAM-I data for heavy nuclei: carbon (circles), oxygen (squares), neon (crosses), magnesium (triangles), silicon (diamonds), and iron (asterisks). The fluxes of the nuclei have been normalized to carbon and a broken power-law, fit to the ensemble, is displayed, along with the indices above and below 200 GeV/nuc.

~ 20 GeV/nuc to $\sim 10^4$ GeV/nuc, resulting in a low-energy index of $\gamma_{\rm LO} = 2.77 \pm 0.03$(stat) and a high-energy index of $\gamma_{\rm HI} = 2.56 \pm 0.04$(stat). The location of the spectral breakpoint is said to be in the range $200 - 250$ GeV/nuc [9], though given the spread in the data and the size of the error bars, it would be interesting to see the results of alternative fits, including single power laws, as well. At 250 GeV/nuc, the CREAM breakpoint for heavy nuclei is possibly in mild conflict with the PAMELA He breakpoint, which, when expressed as an energy per nucleon, is ~ 120 GeV/nuc.

Finally, CREAM data from their third flight were discussed [19]. These data, which are preliminary, are said to be not inconsistent with the above CREAM results. However, they do extend to higher energy and are claimed to contain a hint of a roll-off (softening) above 20 TeV. It remains to be seen whether this roll-off is statistically significant, but such a feature could be a sign of new source component "poking through" the background flux around this energy.

ATIC results were not shown at the conference, but previous results agree reasonably well with CREAM at higher energy, though they undershoot the PAMELA H and He data at lower energy [1]. The ATIC H and He spectra are said to "flatten as energy increases", but a statistical analysis of this has not yet been presented [13].

2.1 Interpretations

The results above, taken together (and modulo some unknown systematic effects), are beginning to tell a story of something being wrong with our baseline standard model of cosmic-ray acceleration and propagation. That model holds that cosmic rays are accelerated by, most likely, supernova remnants through the process of diffusive shock acceleration. One of the central conclusions of this idea, in its simplest form, is that the spectrum of the accelerated particles will follow a power-law in rigidity, with an index determined by the properties of the shock, not of the particles (see, e.g., [20–22]. Hence, all particle species accelerated by the same source should share a common spectral index, and, apart from cutoffs at the upper rigidity extent of the accelerating remnant, these particle spectra should be featureless.

On the other hand, more sophisticated or realistic models, which address, for instance, the back-reaction of the cosmic rays on the shocks, non-planar geometries, time evolution of the system, etc, can generate different results, including concavities in the rigidity spectra and possibly even species-dependent spectral indices [22, 23].

The impact of propagation processes must also be considered. The most common model here is simple diffusion in turbulent Galactic magnetic fields - a rigidity-dependent phenomenon that can alter spectral indices, but which should not induce (sharp) features in the spectra or selectively impact different particle species [24]. More sophisticated treatments should also include spallation effects or convection, or reacceleration processes.

The literature is filled with much excellent work on these topics and it is impossible here to review it all. I will instead concentrate primarily on ideas introduced at the conference to address the particular problem of the flux "anomalies" discussed above. These results again, distilled into bullet form are:

- The p/He ratio drops with energy (i.e., the indices of these elements are different)
- The spectra of p and He break and harden at $R \sim 240$ GV
  - There may be a "dip" in the spectrum prior to the breakpoint
  - The location of the breakpoint for $Z > 2$ may be higher
- The spectra of p and He may soften again above 20 TeV

The ideas discussed at the conference to address these points include new sources, non-uniform distributions of sources, inhomogeneous matter configurations within acceleration sites, variations of "standard" acceleration mechanisms, and more. One of the more popular ideas (likely influenced by the lepton results, discussed below) involved new sources or source classes.

As discussed above, a 3-component model [5] can be fit quite well to the PAMELA data, at least above ~ 10GV[3]. In this model, a new source class — the nova — is introduced to contribute flux at energies below $\sim$ 300 GeV/nuc (supernovae of medium and high-mass stars make up the other two sources classes as in [6]).

A new low-energy component is also discussed by Erlykin and Wolfendale [25, 26], who argue against a nova origin on the basis of energetics and composition. A contribution from highly massive stars with very strong stellar winds (e.g., OB or Wolf-Rayet stars) could resolve both issues, possibly originating from OB associations within the Local Bubble. Two models with local sources were also discussed in [17]. This will be covered in more detail below.

An alternative explanation for differences in the p and He spectra which doesn't invoke new sources or source classes may be revealed by a closer examination of the escape of cosmic rays from their acceleration sites [27, 28]. One idea here involves the so-called "runaway" spectrum of cosmic rays accelerated in, but escaping from a supernova remnant. The spectrum of these particles can, in principle, be different from the spectrum of the particles confined within that remnant. In fact, the runaway spectrum of a particular accelerating chemical species depends not only on the evolution of the maximum acceleration energy, but on the number density of that species in the local environment, as well [29]. Hence, in a region with an inhomogeneous distribution of chemical enrichment, a difference in the spectral index of different species occurs naturally. This is demonstrated schematically in Figure 7, which shows how a depletion in helium density far from an accelerator's center (coupled with a constant H density) can lead to a decreasing p/He ratio with rigidity.

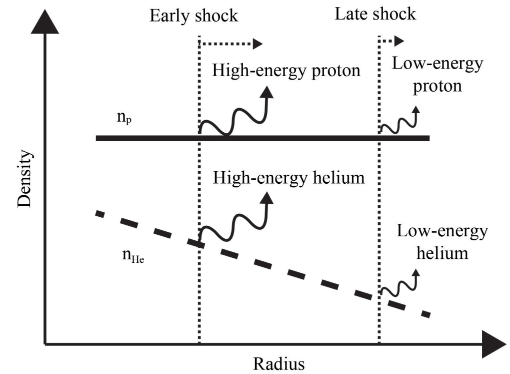

Fig. 7. Schematic diagram demonstrating a possible method to produce differing hydrogen and helium spectra in an inhomogeneous region supporting diffusive shock acceleration [27]. The solid and dashed lines represent the local density of hydrogen and helium, respectively. The thin vertical dotted lines represent the shock front at different times - in the early phase, high-energy cosmic-rays escape, while in the later phase, lower-energy particles escape. In the described configuration, this leads to a p/He to hydrogen ratio which decreases with energy.

In the same paper, spectral hardening was attributed to a decrease in the Mach number with increasing shock radius, which affects all particles of the same rigidity equally [27]. To situate the breakpoint at the proper energy ($E \sim 100$ GeV/nuc), an ambient temperature in the accelerating region of $\sim 10^6$ K is required. It is noted that this condition, as well as inhomogeneities in the chemical abundances may be satisfied in a superbubble environment.

As mentioned above, models of diffusive shock acceleration beyond the test particle limit can introduce features, including concavities, in cosmic-ray spectra. This was discussed in [30], where the hardening of spectra are examined as either the effects of nonlinear shock modification or to distributed re-acceleration of cosmic rays by old supernova shocks, or both. The intrinsic difference between the H and He spectra is explained as the possible effect of a *reverse* shock propagating through, and accelerating particles in, a region depleted of hydrogen — similar to the runaway spectrum model above (see also [31]).

In [32], the spectral hardening was proposed to occur because the cosmic-ray flux at earth is the superposition of spectra from many sources, all of which have a slightly different production spectral index. (See also [33]). The authors note that the effect results in a gradual transition to a harder index, which may be incompatible with the existing data.

Finally, a very comprehensive study of the cosmic-ray data was presented in [17]. Using the GALPROP simulation code [4], the authors construct several models of cosmic-ray injection and propagation and compare the results to measured p & He spectra, boron-to-carbon ratios (see below), antiproton fluxes, diffuse gamma-ray fluxes, anisotropies, and other data (see also [34]).

The models they test include a diffusive-reacceleration reference model tuned to pre-PAMELA results (model R), a model with a local source of high-energy cosmic rays (model H), a model with a local source of low-energy cosmic rays (model L), two alternative source injection models (I), and model featuring only modifications to the propagation parameters (model P).

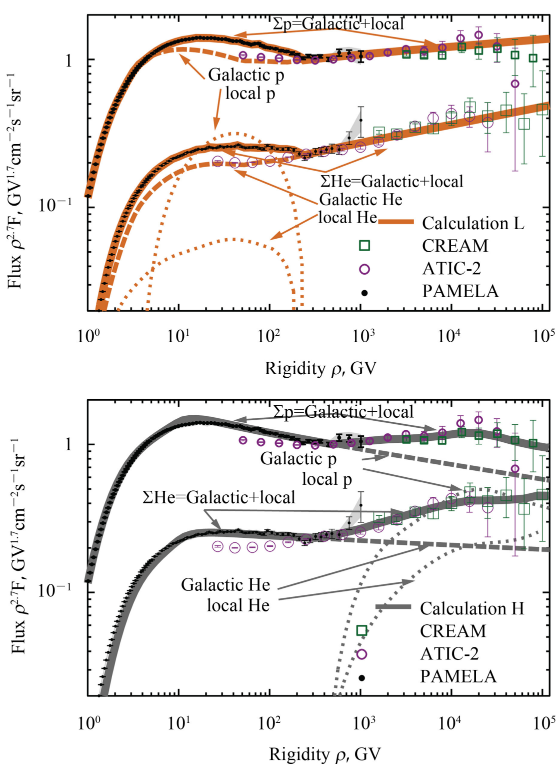

Fig. 8. Cosmic-ray proton and helium data, compared to calculation results. The data are from CREAM, ATIC-2 and PAMELA. The calculations are for two models featuring local sources of cosmic rays - one with high-energy component (H), and one with a low-energy component (L). Local and galactic contributions to the H and He spectra are indicated. Figure from [17].

An example calculation is displayed in Figure 8, which shows a comparison of measured proton and helium fluxes to the H and L models (see also the ratio in Figure 4). The power of using an integrated propagation code like GALPROP is that the same calculation which produces this comparison also makes predictions for other cosmic-ray observables. For instance, the L model, though it can match well the p & He data, overpredicts the anti-proton flux and cosmic-ray anisotropy. Indeed, none of the models tested thus far can reproduce all of the observables, though model P is slightly favored. In this scenario, a change in cosmic-ray transport (reduction of the rigidity dependence of the diffusion coefficient from $\delta = 0.3$ to $\delta = 0.15$) is introduced at 300 GV. This allows it to match most measured data and predicts a testable increase in the B/C ratio at high energy (>1 TeV/nuc) — see Figure 9.

It is worth mentioning that a portion of the modeling here is purely phenomenological - the source spectral indices of p and He, for instance, are adopted *ad hoc* to be different. Thus, while analyses like this provide a very powerful tool for testing the global consequences of differing source and propagation parameters, they don't tell us (nor attempt to tell us) about the internal physics

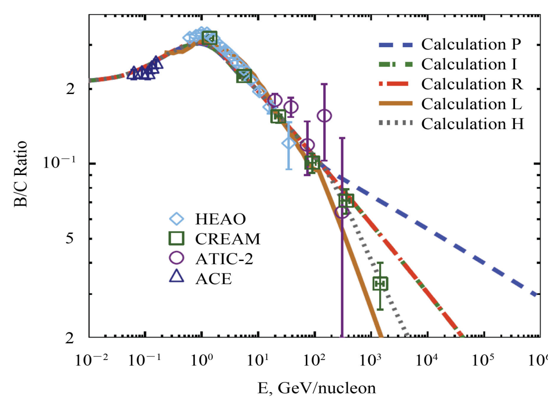

Fig. 9. Flux ratio of cosmic-ray boron to carbon, vs energy, compared to calculation results. Also shown are the results of several calculations, as discussed in the text. Figure from [17].

of *why* the parameters are what they are, as with, e.g., the source models described above. It is therefore important to continue to pursue both lines of research.

3 Heavy ($Z > 2$) Nuclei

Results on heavier nuclei were also presented by several groups. The TRACER (The Transition Radiation Array for Cosmic Energetic Radiation) collaboration [35–37] showed data and final results from their 2006 long-duration balloon flight from Esrange in Sweden. The TRACER instrument uses a suite of detectors, including scintillators, Cerenkov detectors, and a transition radiation array to measure heavy ($Z > 3$) cosmic rays at energies from ~ 1 GeV/nuc to beyond 10 TeV/nuc. Of special note were their results on the elemental spectra of C, O and Fe, all of which were compatible in the high-energy region ($E >\sim 20$ GeV/nuc) with a single power-law of index 2.65. No evidence of spectral hardening at ~ 200 GeV/nuc is reported.

In addition to the primary species data, TRACER showed their final results on the flux ratio of boron to carbon. This ratio is of particular interest for the modeling of cosmic-ray propagation, because boron is thought to be produced purely as a secondary particle. Therefore, any boron detected in the cosmic-ray flux was produced by the spallation during propagation of parent nuclei (mostly carbon), and hence the abundance ratio is a direct measure of the overall propagation history of the particles. The data, shown in Figure 10, feature the highest-energy measurements yet obtained for this ratio (at $E \sim 2$ TeV/nuc). The results have been fit using a Leaky-Box [38] formalism where the propagation history is parameterized using an energy-dependent escape pathlength, $\Lambda_{\rm esc} \propto E^{-\delta} + \Lambda_0$. The result of the fit (which here is to all B/C data) is $\delta = 0.64 \pm 0.02$ and $\Lambda_0 = 0.7 \pm 0.2$ g/cm^2. The constant term here represents a residual or minimum pathlength that all particles must propagate through, possibly in some high-density source region.

As the figure shows, a non-zero Λ_0 pulls the B/C ratio upwards and ultimately flattens it out to a constant value at high energy. This potentially makes it degenerate below ~ 10 TeV/nuc with the predictions of the P scenario described above (see Figure 9). Interestingly, a non-zero Λ_0 also has the effect of inducing an upturn (hardening) in the energy spectra of the primary elements - though at energies higher than those discussed in the previous section, beyond ~ 1000 GeV/nuc.

Unfortunately, because there is little B/C data at high energy, there is still considerable uncertainty in the results of the fits. The error contours shown in [36] appear flat enough to allow, for instance, $\delta = 0.55$ and $\Lambda_0 = 0$ g/cm^2, similar to what was found in [39]. Higher B/C statistics in the 100-1000 GeV/nuc range are crucial to clarifying this issue. Other direct measurements of heavy nuclei were presented by the CRIS (Cosmic Ray Isotope Spectrometer) team. This instrument, which uses a stack of silicon detectors to apply the dE/dx vs. $E_{\rm tot}$ method, can measure isotopic abundances to energies up to ~ 500 MeV/nuc [40]. CRIS has obtained an impressive 14-year exposure on board NASA's Advanced Composition Explorer satellite. Even with a relatively modest geometric factor, CRIS has amassed more than 100 m^{2}sr-days of exposure, which puts it on par with the largest balloon instruments flying today.

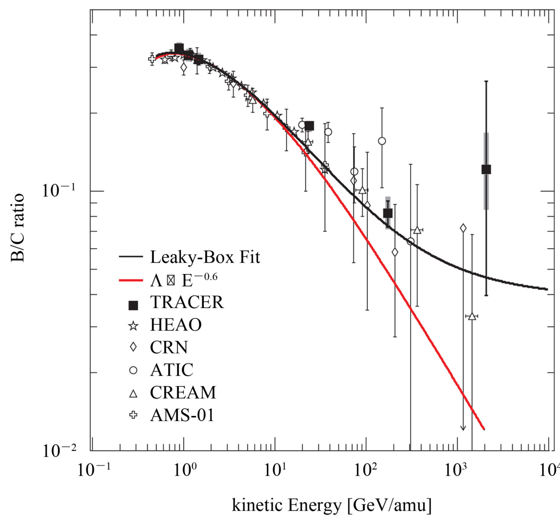

Fig. 10. Ratio of the flux of cosmic-ray boron to carbon vs kinetic energy, as measured by the TRACER instrument. The TRACER data points are indicated by filled squares and display separate statistical and systematic errors (lines and shaded bars, respectively). Also shown are data from several other balloon and space instruments, (symbols as labeled - see [36] for citations). The two lines represent the results of two leaky-box propagation calculations. The red line shows simple a priori model with $\delta = 0.6$ and the black line represents a fit to all data with a residual pathlength model (see text for more details).

In [41], CRIS measurements of the ultra-heavy nuclei $_{31}$Ga and $_{32}$Ge were presented. The isotopic cosmic-ray abundances of these nuclei have never been measured before. In addition, greatly improved abundances for $_{29}$Cu and $_{30}$Zn were shown. In all cases, the data are consistent with a composition consisting of 80% solar-like material and 20% massive star outflow (though it is noted that these isotopes lack the strong discriminating power of, e.g., $_{22}$Ne or

$_{58}$Fe). As shown in Figure 11, the CRIS data, on-whole, support well an OB-Association/Superbubble model of cosmic-ray origins, as discussed in [42] and [43] (see also [44]).

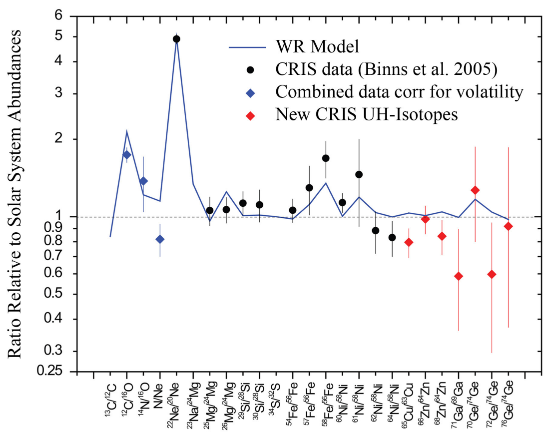

Fig. 11. Comparison of the CRIS isotopic cosmic-ray measurements vs the WR (Wolf-Rayet) model in which abundances are assumed to consist of a mixture of 80% solar-system-like material with 20% massive-star outflows [41]. See text for details.

In the same session Labrador et al. [45] discussed new methods which allow for the analysis of higher-energy particles which completely penetrate the CRIS detector stack. These techniques may extend the energy reach of the instrument to as high as $\sim$ 800 MeV/nuc for some elements (iron was demonstrated).

The PAMELA team also presented results on their efforts to enable isotopic measurements of light nuclei using their instrument [46, 47]. Studies employing both the velocity vs. rigidity technique and a multiple dE/dX technique were introduced, along with nice preliminary results on the D/$_3$He ratio from $\sim$ 150 MeV/nuc - $\sim$ 1 GeV/nuc. Very preliminary results on the ^{7}Li/^{6}Li, ^{10}Be/^{9}Be, and ^{7}Be/(^{9}Be+^{10}Be) near 1 GeV/nuc were also shown. Methods of isotopic separation using geomagnetic fields were explored in [48].

4 Electrons

Cosmic-ray electron measurements have long been valued for the unique insights they provide into our local interstellar environment. Due to rapid (dE/dt $\sim E^{-2}$) energy losses from synchrotron radiation and inverse Compton scattering, electrons at high energy have a restricted diffusion radius ($R \sim 300(E/\text{TeV})^{-0.35}$ pc [49]) and hence detailed observations of their flux probe local propagation conditions, and may reveal the existence of nearby recent cosmic-ray sources.

Electron measurements have been much discussed in recent years, driven by new data and conflicting claims of sharp or smooth features in the energy spectrum [50]. These features (which are closely tied to the positron measurements discussed in Section 5) have been attributed to a host of phenomena, including dark matter decay, nearby pulsar emission, and more prosaic propagation physics. See, e.g., [51, 52] for a review and list of publications. Of specific interest are claims of a sharp peak in the electron spectrum at 300-800 GeV, measured by the ATIC-2 collaboration [53], which have not been verified by measurements from Fermi and H.E.S.S.

Results on the electron spectrum, as measured by the Large Area Telescope (LAT) of the *Fermi Gamma-ray Space Telescope* were presented [54]. The LAT is a pair-conversion telescope designed to measure gamma rays in the energy range $\sim$20 MeV to $>$ 300 GeV. It features a silicon/tungsten tracker system followed by a segmented hodoscopic 8.6 radiation-length deep CsI electromagnetic calorimeter. It is surrounded by a hermetic charged particle veto system. The instrument was launched in June, 2008 and has a peak effective geometric factor for electron measurements of $\sim$2.8 m^{2}sr at 50 GeV [55].

As an electron measuring device, the LAT essentially looks for gamma-ray-like events which have hits in the veto system. However, because the instrument lacks an intrinsic charge discriminating device (though see Section 5 below), it must overcome a large background of proton events, which outnumber the electrons by a factor of 10^2 or more, increasing with energy. This is achieved through a series of hadron-rejection cuts, based on differences in the morphology of electron and hadron events in the various detector subsystems. A key component of this procedure is exploiting the difference in the profiles of the electromagnetic shower in the imaging calorimeter. In simple terms, hadronically-induced showers tend to be wider. By cutting on the lateral profile width and other variables, a claimed rejection power of 10^3 at 200 GeV is obtained, rising to 10^4 at 1 TeV [56]. More or less the same methods are employed with the imaging calorimeter devices on ATIC and PAMELA as well.

Even after these cuts are applied, however, there exists a residual background of "electron-like" proton events (e.g., protons which convert most of their energy into a π^0 in their first interaction in the instrument), which can exceed 20% at high energy [55].

These events must be corrected for in the final determination of energy spectra.

The Fermi/LAT team presented an update to their all-electron energy spectrum published on 12 months of data in [55]. The new results, which are still preliminary, include 29 months of observations, and cover the energy range ~ 40 GeV to ~ 1 TeV. Figure 12 shows the resulting weighted energy spectrum to be in excellent agreement with the previous data. Those data could be fit with a power-law of index 3.08 ± 0.05. No "prominent" spectral features were found, but a "slight" hardening and subsequent softening (at 100 GeV and 500 GeV, respectively) could not be excluded.

Because the reconstructed output spectrum requires a correction factor to account for residual hadronic contamination, inaccuracies in the assumed underlying proton flux could lead to errors in the final results. In particular, an additional flux of misidentified high-energy protons due to spectral hardening at a ~ 100 GeV could, in principal, lead to harder measured electron spectra. This effect was tested by the LAT team and was found to be small compared to the overall systematics of the measurement.

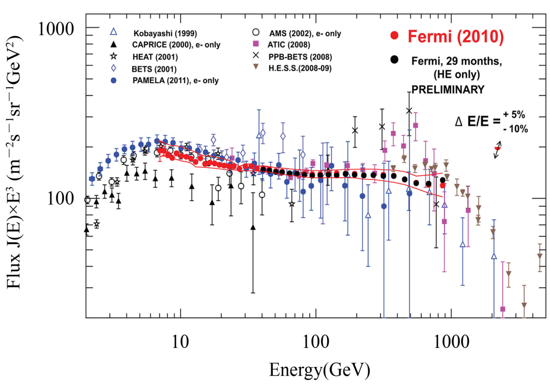

Fig. 12. Cosmic-ray all-electron flux, as measured by the Fermi LAT. The flux from 7 GeV to 1 TeV, as published in [55], is shown in red, along with the updated preliminary analysis of high-energy (E>20GeV) data from over 29 months of data (in black) [54].

The team also reported on continuing work underway which will enhance the energy resolution of the LAT at high energy by selecting only those events which traverse a longer pathlength through the instrument (12 X_0 vs 7 X_0, where X_0 is the radiation length). This approach improves the energy resolution from $\sim 15\%$ to $\sim 5\%$ at high energy and promises to increase the upper energy range of measurement from 1 TeV to ~ 3 TeV. The improvement in energy resolution may be important to reveal any possible structure in the high-energy spectrum, while the extended energy reach can address claims of a spectral cutoff, as reported by the H.E.S.S team [57].

The PAMELA collaboration also presented cosmic-ray electron results [58]. The data, which were published very recently [59] come from a 1200-day exposure and cover the energy range of 1 GeV to 625 GeV. Because it is a spectrometer, PAMELA can isolate negatively charged particles, so unlike the LAT results discussed above, this is a pure negative electron measurement. As can be seen in Figure 13, given the statistical and systematic uncertainties, the data are consistent with the results of the LAT, and can be described by a power-law with an index of 3.18 ± 0.05 above 30 GeV [60]. A lack of statistics at high energy limits the ability to test the existence a possible feature in the spectrum at $\sim 300 - 800$ GeV [53].

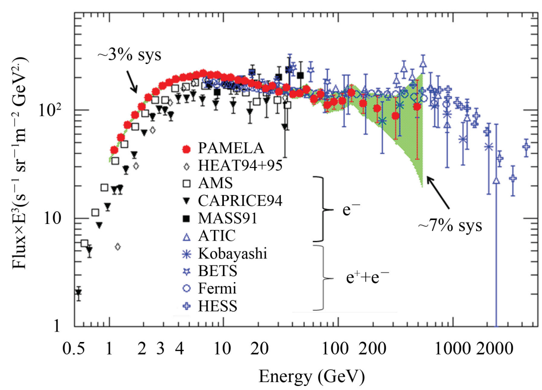

Fig. 13. PAMELA measurements of the cosmic-ray electron (e^- only) flux, from 1 GeV to 625 GeV [58]. The PAMELA data are shown with filled red circles, compared to other recent data (see [59] for references). The green shaded zone represents the systematic uncertainty in the measurement, which increases from $\sim 3\%$ at low energy to $\sim 7\%$ near 600 GeV.

The design of PAMELA allows for two independent energy-determination methods to be applied. One uses the rigidity obtained from the spectrometer and one uses the reconstruction of electromagnetic cascades in the calorimeter. These are found to be in good agreement and can be used to place a 2% systematic error in the overall electron spectrum energy scale.

Interestingly, despite having spectrometric information, mis-reconstructed ("spillover") protons represent a substantial background to the electron measurements at high energies, reaching as high as x10 the electron flux at 500 GeV [59]. This background, however, can be effectively rejected by requiring electron-like interactions in the calorimeter. This is similar to the procedure performed by the LAT team, but given the smaller initial contamination level, results in a negative electron sample which is effectively pure up to ~ 600 GeV.

An indirect ground-based observation of high-energy electrons was also presented at the conference by the MAGIC team [61]. MAGIC (Major Atmospheric Gamma-ray Imaging Cherenkov Telescope) is a pair of 17m imaging atmospheric Cerenkov telescopes located in LaPalma, one of the Canary Islands. Using essentially the same technique as the H.E.S.S. collaboration has employed [57], the MAGIC team reported on preliminary measurements of the high-energy cosmic-ray all-electron spectrum from 100 GeV to 3 TeV. The results, shown in Figure 14, are compatible with previous work and can be fitted with a power law of slope $3.16 \pm 0.06(\mathrm{stat}) \pm > 0.15(\mathrm{sys})$.

As with the direct measurements above, hadron rejection is an essential component of the MAGIC method. Indeed, the current limiting factor in the analysis is the availability of the Monte Carlo simulations needed to evaluate the level of background contamination by misidentified heavy cosmic rays. With more simulations, a substantial increase in statistics should be possible. Also, because of its large mirror area, and subsequently low energy threshold for air shower detection, MAGIC should, in principle, be able to extend measurements to below 100 GeV.

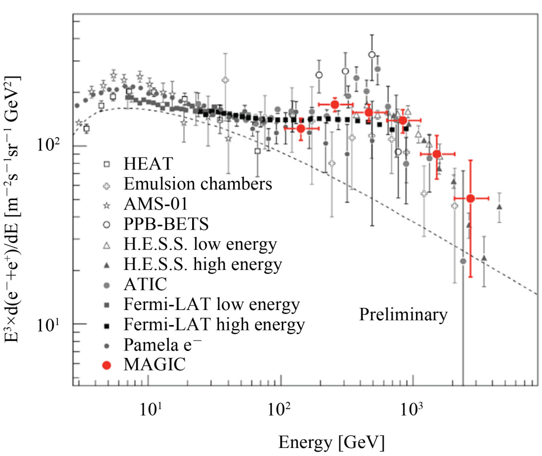

Fig. 14. Preliminary cosmic-ray all-electron spectrum, as measured by the MAGIC imaging atmospheric Cerenkov array.

In addition to the above measurements, final results were presented from the longstanding balloon-borne emulsion chamber program of Nishimura et al. [62]. A energy spectrum derived from an 8.2 $\mathrm{m^2}$sr-day exposure, collected in 15 balloon flights over 33 years was presented. The spectrum, which extends from 30 GeV to 3 TeV, can be fitted with a power-law of 3.28 ± 0.10. Any cutoff, should it exist, is at energies above 1.9 TeV, at 90% confidence level.

4.1 Interpretations

At mentioned at the start of this section, a large body of work has been developed lately in an effort to describe the shape of the electron spectrum, as we currently measure it. It is clear that conventional propagation models tuned to pre-Fermi data sets tend to feature softer, largely featureless, spectra which do not match the latest data (see, e.g., dotted line in Figure 14). Whether the resolution to this lies in modifying/improving our models of propagation, or in updating our assumptions about the distribution of electron sources (or both - or neither!) remains to be seen.

Several groups presented work on this problem, most of which concentrated on possible new sources of electrons. A generic high-energy hard-spectrum $e^+ + e^-$ source was discussed in [54] as a way to simultaneously match the curvature in the electron spectrum and the upturn in the positron fraction (see below). Identifying observable signatures for differentiating between various astrophysical or exotic models is, of course, the subject of much study right now. The behavior of the electron spectrum or positron fraction at high energy is clearly an important part of this (e.g., [52, 63]).

One model combining a distribution of distant and old primary electron and positron sources with young nearby sources was described, which is noteworthy for its prediction of a positron fraction which levels off to ~ 0.22 above 100 GeV [64]. The impact of a small number of local sources was also examined in [65], specifically with reference to putative "fine structure" in the ATIC-2/ATIC-4 electron spectrum. Other authors explored the contribution of specific sources, including Vela-X [66], or the Galactic Center region [67]. The important connection between measured Galactic synchrotron emission and the low-energy electron flux was pointed out as well [68].

5 Antiparticles

In the absence of primary sources, the standard model for the origin of cosmic-ray antiparticles (e^+, $\bar{p}$) is secondary production due to interactions of cosmic rays propagating in the interstellar medium. This leads to antiparticle fractions which, like the boron-to-carbon ratio, tend to drop at high energy [17], as shown, for example, by the model line on Figure 15.

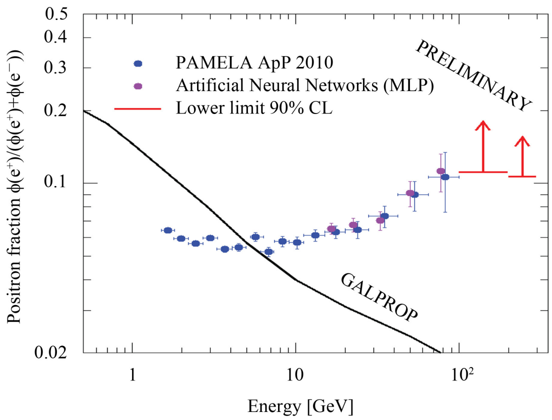

Fig. 15. The cosmic-ray positron fraction ($e^+/(e^-+e^+)$), as measured by the PAMELA instrument [58]. Previously-published results [70] are shown with blue symbols; new preliminary results featuring an alternative analysis method are shown in magenta. New preliminary 95% CL lower limits to the positron flux are shown in red. A standard secondary production model calculated using GALPROP is shown in black.

As mentioned in the previous section, "anomalies" in the measured positron fraction ($e^+/(e^-+e^+)$, coupled with "features" in the electron spectrum, have led to much work and speculation. The rising positron fraction reported by PAMELA [69] (see Figure 15) has, in particular, been of great interest. In a follow-up to these results, the PAMELA team presented their latest data on the flux of cosmic-ray positrons [58]. The updated work is a re-analysis of the existing positron fraction results, and uses a neural network event classifier applied to candidate events above ~ 15 GeV. The results, which are preliminary, agree quite well with their previously published data and can be extended to somewhat higher energies.

Rather than quoting firm fractions, however, the team has taken a conservative approach and varied all systematics in such a way as to generate a 90% confidence-level lower limit to the positron fraction above 100 GeV. This is shown in Figure 15, where it can be seen that the fraction does not drop significantly above 100 GeV, and may, in fact, continue to rise.

The primary background for positron measurements is proton contamination. Since the p/e^+ ratio is $\sim 10^4$ at 100 GeV, this requires very robust hadron rejection techniques. The standard method for discriminating between these events is by examining the transverse and lateral shower profiles in the calorimeter. These methods become less efficient around 100 GeV, so the PAMELA team has explored new methods [71] of extending this beyond 300 GeV. Note that an independent method for providing lepton/hadron separation in such experiments (e.g., HEAT [72] or AMS (see below)) is a transition radiation detector, which is sensitive to particle Lorentz factor and hence can differentiate between light and heavy particles at a fixed energy.

The positron fraction can be used, along with the all-electron spectrum, to generate an estimate of the positron flux alone. This is shown in Figure 16, along with previous measurements.

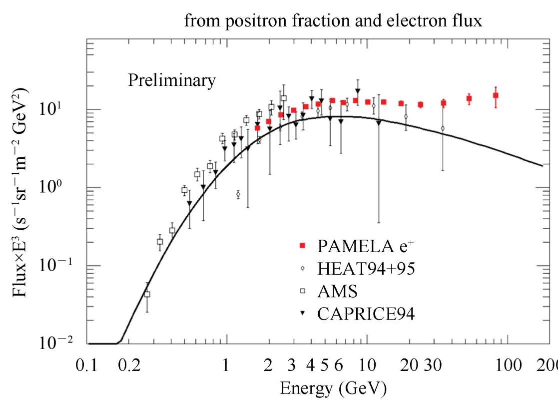

Fig. 16. The preliminary cosmic-ray positron flux, as measured by PAMELA.

As previously mentioned, the Fermi/LAT instrument lacks an intrinsic charge-sign discrimination device, and hence cannot, without some external influence, measure electrons and positrons separately. That influence can, however, be introduced by employing the earth's magnetic field as a charge separator [73]. This idea was proposed in [74] and pioneered on a balloon platform in [75].

The basic idea is that, because of the magnetic field of the earth, certain trajectories can be forbidden for particles of a given rigidity. This defines, for an orbital period, a westward-facing region where, for a range of rigidities, only positrons should be detectable. An eastward-facing "electron-only" region can likewise be defined — see Figure 17.

By continuously tracking the instantaneous detector position and carefully tracing particle trajectories through a precise model of the earth's magnetic field, the team is able to selectively collect positrons and electrons. A north-south "control" region is also defined, which includes particles of both species. The final results, which range from 20 GeV to 200 GeV, are shown in Figure 18, expressed as a positron fraction. The data are in good agreement with the previous PAMELA results, and indicate a positron fraction

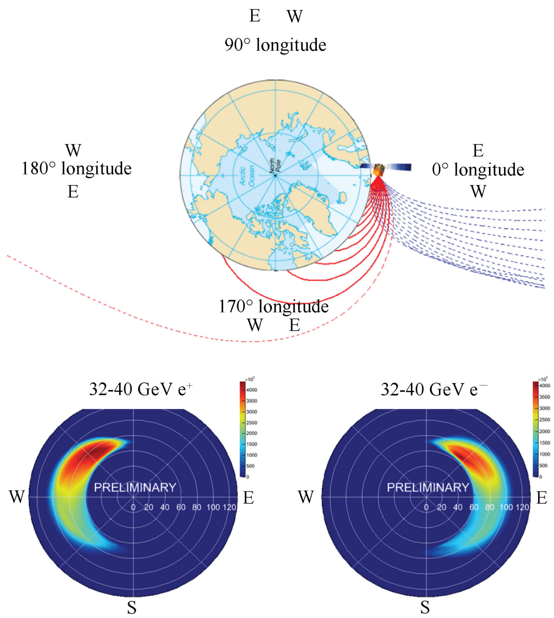

Fig. 17. Top Panel: Schematic view of particle trajectories in the earth's magnetic field. Here allowed trajectories of positrons are shown in blue and forbidden trajectories of electrons are shown in red. Bottom Panel: Exposure maps for positrons (left) and electrons (right), in the energy range 32-40 GeV. Images from [73].

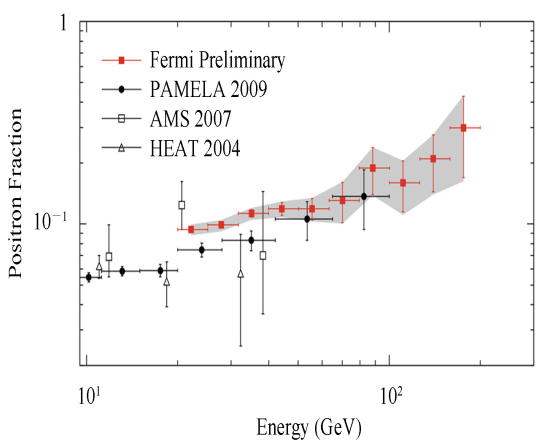

Fig. 18. Preliminary positron fraction, as measured by the Fermi Large Area Telescope. Also shown are results from several other experiments. The error bars on the LAT points are statistical, while the gray shaded region represents the systematic uncertainties.

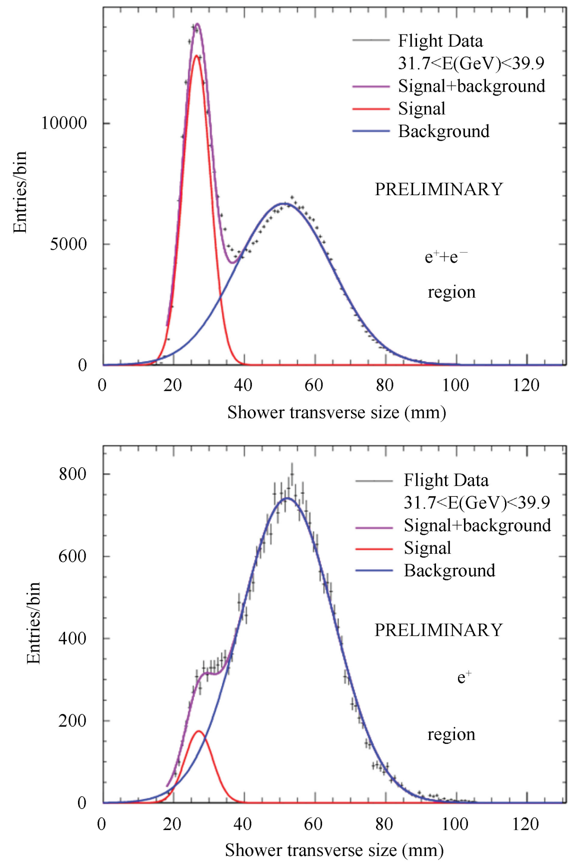

Fig. 19. Shower transverse size distributions for signal and background populations for the LAT positron measurement. The blue line represents a background of misidentified protons. The red line represents "signal" — either a mixture of positrons and electrons from the control region (top panel) or positrons alone from the western-facing region (bottom panel).

which continues to rise. There may be some disagreement with the PAMELA results below ~ 30 GeV, where the LAT results seem systematically higher.

As above, the rejection of the proton background, which exceeds the positron flux by a factor of up to $\sim 10^4$, is achieved by analysis of the shower morphology in the calorimeter. However, given the depth of the LAT calorimeter, even with very hard cuts, the residual proton contamination can be substantial (see Figure 19). Confidence that the background subtraction has been done properly is achieved by employing both a Monte Carlo and a data-fitting method.

Another technique designed to exploit the earth's magnetic field for spectroscopy was presented in [76]. The general concept here, as first discussed in [77], is to probe particle and antiparticle fluxes by using the rigidity-dependent shadow cast in the cosmic-ray flux by the Moon†. In particular, the authors propose to use the MAGIC imaging atmospheric Cerenkov telescope (IACT) to measure the positron/electron flux ratio at $\sim 300-700$ GeV. The challenge here (apart from hadron rejection) is to identify electron-like showers in the close vicinity of the Moon. As shown in Figure 20, the angular separation between the moon and the shadow of ~ 400 GeV electrons is roughly 4°, which limits observations to periods when the moon is $< 50\%$ full, and which requires a special reduced-gain observing mode for other bright phases.

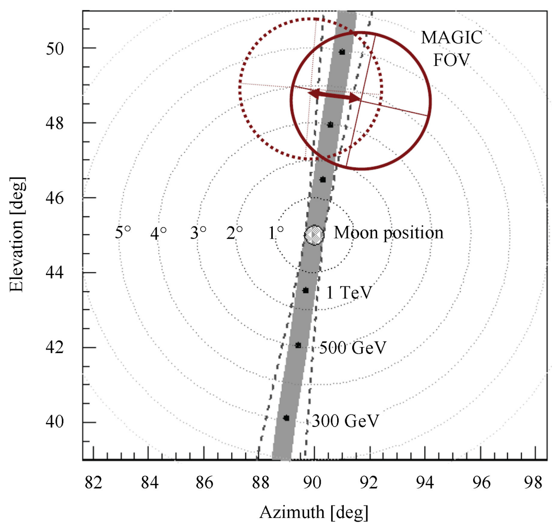

Fig. 20. Location of the Moon shadow for electrons at different energies. In this figure, the electron shadow would appear below the moon position (eastward) and the positron shadow would occur above the moon (westward). The dashed lines represent the uncertainty in the possible shadow location due to imperfect knowledge of the geomagnetic field. The red circles show the field-of-view of the MAGIC telescopes, in a possible observing strategy which wobbles around the shadow position.

After excluding high-zenith angle ($\theta >\sim 50°$) pointings (for which the energy threshold is too high), and bright-phase periods (as defined above), the MAGIC team anticipates that roughly 40 hours of observing time are available each year for these measurements. Depending on the actual particle flux above 300 GeV, this would allow for a measurement of the positron fraction with a few years of observations.

5.1 Antiprotons

The flux of antiprotons has played an important role in constraining models of particle origins and propagation (see Section 2). The good agreement between measured data and standard secondary production models above 10 GeV, for instance, has posed a challenge to some dark matter explanations of the excess positron flux [79]. At lower energy, antiproton data provide useful insights into solar modulation, and the effects of convection and reacceleration in particle transport.

A measurement of the antiproton spectrum from 0.17 to 3.5 GeV was presented by the BESS-Polar II team [80]. BESS, the Balloon-borne Experiment with a Superconducting Spectrometer, is a large high-resolution spectrometer which employs a thin superconducting solenoid magnet of 0.8T, combined with internal and external drift-chamber trackers, a hodoscopic time-of-flight system, and an aerogel Cerenkov detector. The so-called "Polar" configuration of the instrument has a maximum detectable rigidity of 270 GV and a geometric factor of 0.23 m^{2}sr. The BESS-Polar II payload had a 24.5-day flight from Antarctica in December of 2007, during solar minimum. As shown in Figure 21, the measured flux is completely consistent with models of pure secondary production, and provides no support for contributions

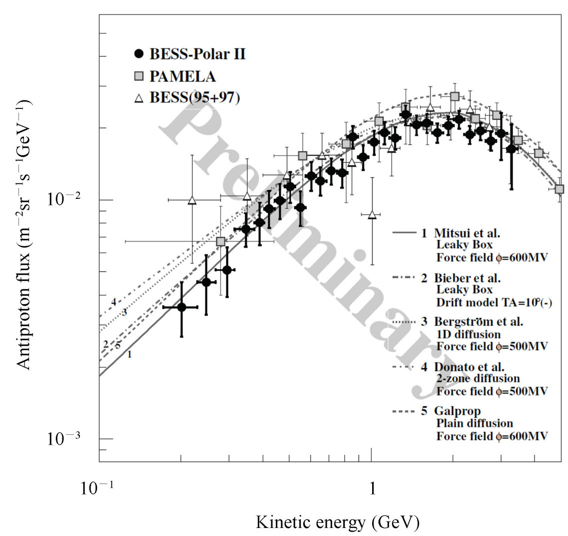

Fig. 21. Preliminary low-energy antiproton flux, as measured by the BESS-Polar II payload. Also shown are measurements from the PAMELA payload and previous BESS flights. Several models of secondary antiproton production are also shown.

†A similar approach, used to set a limit on the antiproton/proton ratio at ~ 5 TeV with the ARGO-YBJ detector, was discussed in the HE1 sessions [78].

from more exotic sources, such as primordial black hole evaporation or dark matter annihilation.

At lower energies, the PAMELA team also presented the first ever detection of geomagnetically-trapped antiprotons [81]. These particles, which have been predicted to exist as a radiation belt surrounding the earth, are created during interactions of cosmic rays with the earth's atmosphere, and are subsequently trapped within its magnetosphere. The PAMELA results, spanning the energy range 60-750 MeV, prove not only that this belt exists, but that it contains antiproton fluxes some 10^3 times larger than the cosmic-ray antiproton flux, making it the most abundant source of antiprotons near earth.

6 New Experiments and Instrumentation

More than 20 papers were presented at the conference covering new experiments, techniques, and instrumentation. The subjects spanned a range of topics, from a study of albedo produced in cosmic ray/lunar regolith interactions [82], to a pinhole camera technique for imaging ultra-high-energy cosmic rays [83], to a review of NASA's super-pressure (ultra-long-duration) balloon program [84].

A major new project which was discussed in several papers is the CALorimetric Electron Telescope, CALET (see [85] and [86] for an overview and additional citations). CALET is a space-based mission which is scheduled for deployment to the International Space Station in 2013. It will comprise a charge detector, a 3 radiation-length (r.l.) deep imaging Tungsten/SciFi (scintillating fiber) calorimeter, and a 27-r.l. deep "total absorption calorimeter" made of coarse segmented lead tungstate crystals — see Figure 22.

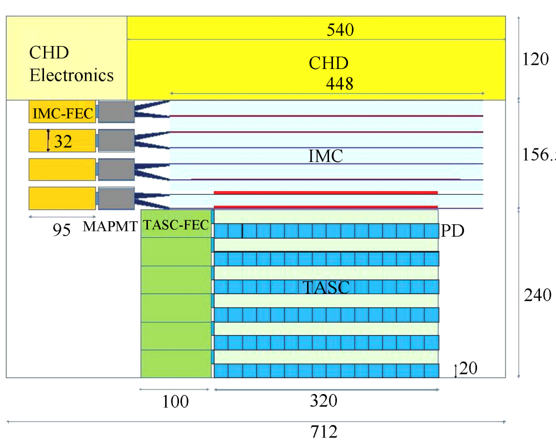

Fig. 22. Schematic diagram of the proposed CALET payload. The main components are a charge detector system (CHD), a thin imaging calorimeter (IMC), and a total-absorption calorimeter (TASC).

The CALET detector has been in development for several years and has already had two successful prototype balloon flights [87]. The overall design has gone through a few iterations, with the latest version descoped somewhat to reduce technical and schedule-related risks. The new geometric factor is ~ 1200 cm^{2}sr for electrons. This is roughly 6 times smaller than previous versions, though the impact of this has been partially offset by an increased mission lifetime (5 years vs. 2 years) [50].

Though CALET will be much smaller than the LAT (0.12 vs. 2.8 m^{2}sr), it is designed specifically to measure high-energy electrons, and hence has some advantages over the LAT. Some of these advantages stem from the depth of the calorimeter, which is 30 radiation lengths deep, vs. 10.1 ($1.5X_0$ for tracker, $8.6X_0$ for calorimeter) for the LAT. A deeper calorimeter (i.e, the total-absorption calorimeter) provides better energy resolution ($\sim 2\%$ vs. $7-10\%$, above 100 GeV), and improved hadron rejection ($\sim 10^5$ vs $\sim 10^3$) [88].

The charge detector on CALET is designed to have excellent ($\mathrm{d}Z \sim 0.15$) charge resolution for light elements. This should allow it to make useful measurements of, for instance, boron-to-carbon to energies exceeding 1 TeV/nuc — see Figure 23. The addition of a veto counter makes CALET an effective gamma-ray measuring instrument as well.

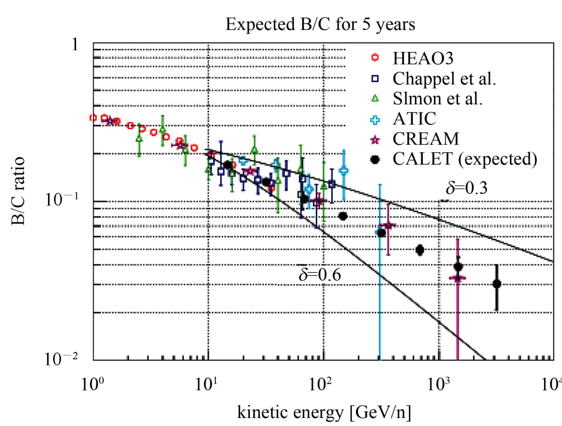

Fig. 23. Simulated boron-to-carbon ratio for a 5-year exposure of the CALET instrument, assuming a diffusion coefficient with power-law index of $\delta = 0.45$ [86].

A similar electron-measuring instrument, TANSUO (Chinese for "Exploration"), was also described

[89, 90]. TANSUO is envisioned as a 34.5 radiation-length deep (total depth), 5000+ cm^{2}sr electron telescope with a Bismuth Germanium Oxide (BGO) calorimeter to be launched by the Chinese space agency in late 2015.

Several presentations were also made by the Super-TIGER (Trans-Iron Galactic Element Recorder) team ([91] and citations therein). Super-TIGER is a follow-up to the very successful TIGER payload, which was designed to study the origins of galactic cosmic rays by measuring the detailed abundances of ultra-heavy ($Z > 30$) elements in the flux. TIGER had several successful flights resulting in ~ 20 m^{2}sr-days of exposure.

Super-TIGER, shown in Figure 24, will feature two independent detector modules, each comprising a scintillator and hodoscope array, coupled to a pair of Cerenkov detectors - one acrylic and one aerogel. Each module is twice the size of the original TIGER instrument, for a total active area of 5.4 m^2. Super-TIGER is scheduled to have its first long-duration balloon flight in 2012.

Finally, a status update was delivered on a major new instrument, the Alpha Magnetic Spectrometer (AMS-02), which was launched by the space shuttle on May 16, 2011 [92]. AMS-02 is a magnet spectrometer instrumented with a transition radiation detector (TRD), a time-of-flight system (TOF), a ring-imaging Cerenkov detector (RICH), and an electromagnetic calorimeter. The tracking system of the spectrometer is built around 9 layers of silicon microstrip detector.

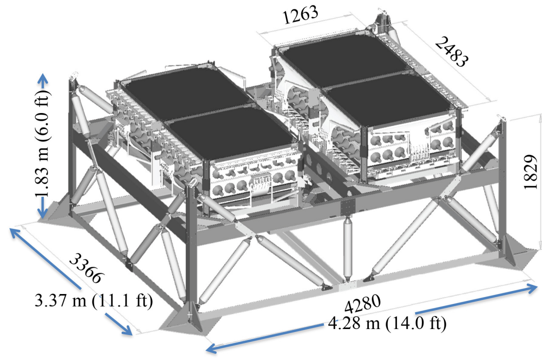

Fig. 24. Diagram of the Super-TIGER ultra-heavy cosmic-ray detector, which features two independent detector modules for a total effective area of 5.4 m^2 [91].

Under design since ca. 2000, AMS-02 was originally constructed to employ a superconducting magnet as the core of its spectrometer. In 2010, the instrument was reconfigured to instead use the permanent magnet of the original AMS-01 mission, which flew on the space shuttle in 1998. The new magnet has a lower field (~ 0.14T) than the planned superconducting magnet (~ 0.8T), so to maintain a high MDR of 2.2 TV, the tracking system has been reconfigured to increase the lever arm over which particle trajectories are measured [93, 94]. An additional layer has been added and 2 layers have been moved to positions further from the center of the bore — see Figure 25.

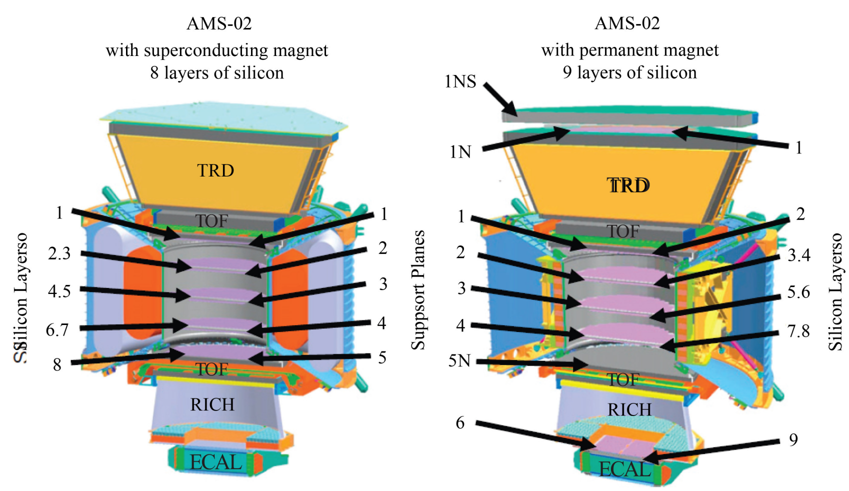

Fig. 25. Schematic of the original and current design of AMS, the Alpha Magnetic Spectrometer, taken from [94]. The new design uses the AMS-01 permanent magnet and relocated tracking detectors, as indicated on the diagram. See text for details.

The geometric factor of the new configuration is said to be largely unchanged for rigidities up to 400 GV [94], while above this point, it is reduced by a factor of 1.5-2.0, putting it in the range of $\sim 0.3\ \mathrm{m^2 sr}$ [95]. Results from AMS-02 on virtually all of the observational targets discussed above are eagerly anticipated.

7 Conclusion

At the risk of sounding clichéd, these are exciting times in cosmic-ray physics. New high-precision results on a number of important topics are emerging which stand to change many of our existing ideas on the nature of cosmic rays. To paraphrase a comment overheard at one of the sessions - it seems as though the data are pushing us into a new era, where our first-order models of cosmic-ray origins are no longer sufficient. On the other hand, given the difficulty in making and interpreting these measurements, it is only prudent to retain a healthy measure of skepticism in our consideration of the results. Forthcoming data from AMS-02 will have much to contribute on these topics and I look forward to the 2013 ICRC, where presumably we will see some of its initial results.

I'd like to thank the scientific organizers for the invitation to give this rapporteur talk, as well as the local organizing committee for excellent help in collecting talks and printing papers. I'm also grateful to Dietrich Müller, Martin Pohl, Joerg Hoerandel, and Nahee Park for useful comments in producing the talk and paper.

References

[1] O. Adriani, et al., 2011, Science, 332, 69
[2] A. Karelin, et al., 2011, ICRC, 6, 6
[3] C. Marco and P. Picozza, 2011, ICRC, 6, 97
[4] A. W. Strong and I. V. Moskalenko, 1998, ApJ, 509, 212
[5] V. I. Zatsepin and N. V. Sokolskaya, 2006, A&A, 458, 1
[6] P. L. Biermann, 1993, A&A, 271, 649
[7] E. S. Seo, 2011, ICRC (highlight), in press
[8] Y. S. Yoon, et al. 2011, ApJ, 728, 122
[9] H. S. Ahn, et al. 2010, ApJ, 714, L89
[10] K. Asakimori, et al. 1998, ApJ, 502, 278
[11] I. P. Ivanenko, et al., 1993, ICRC, 2, 171
[12] J. P. Wefel, et al., 2005, ICRC, 3, 105
[13] J. P. Wefel, et al., 2008, ICRC, 2, 31
[14] A. D. Panov, et al., 2009, Bull. Russ. Acad. Sci. Phys., 73, 564
[15] V. A. Derbina, et al., 2005, ApJ, 628, L41
[16] M. Aguilar, et al., 2002, Phys. Rep., 366, 331
[17] T. A. Porter, 2011, ICRC, 6, 193
[18] J. Alcaraz, et al., 2000, Phys. Lett. B, 494, 193
[19] Y. S. Yoon, 2011, ICRC, 6, 90
[20] L. O'C Drury, 1983, Rep. Prog. Phys., 46, 973
[21] M. G. Baring, 1997, Very High Energy Phenomena in the Universe, Moriond Workshop, 97
[22] M. A. Malkov and L. O'C Drury, 2001, Rep. Prog. Phys., 64, 429
[23] D. C. Ellison, L. O. Drury and J. P. Meyer, 1997, ApJ, 487, 197
[24] A. W. Strong, I. V. Moskalenko and V. S. Ptuskin, 2007, Annu. Rev. Nucl. Part. Sci., 57, 285
[25] A. Erlykin, 2011, ICRC, 6, 213
[26] A. Erlykin, 2011, ICRC, 6, 140
[27] Y. Ohira, 2011, ICRC, 6, 201
[28] L. Drury, 2011, ICRC, 6, 170
[29] Y. Ohira and K. Ioka, 2011, ApJ, 729, L13
[30] V. Ptuskin, 2011, ICRC, 6, 234
[31] M. Pohl, 2011, ICRC, 6, 136
[32] Q. Yuan, 2011, ICRC, 6, 217
[33] Q. Yuan, B. Zhang and X.-J. Bi, 2011, Phys. Rev. D, 84, 043002
[34] A. E. Vladimirov, et al., 2012, ApJ, 752, 68
[35] P. J. Boyle, 2011, ICRC, 6, 51
[36] A. Obermeier, 2011, ICRC, 6, 39
[37] D. Muller, 2011, ICRC, 6, 71
[38] R. Cowsik, et al., 1967, Phys. Rev., 158, 1238
[39] H. S. Ahn, et al., 2008, Astropart. Phys., 30, 133
[40] E. C. Stone, et al., 1998, Space Sci. Rev., 86, 285
[41] W. R. Binns, 2011, ICRC, 6, 25
[42] J. C. Higdon and R. E. Lingenfelter, 2003, ApJ, 590, 822
[43] W. R. Binns, et al., 2005, ApJ, 634, 351
[44] M. Israel, 2011, ICRC, 6, 28
[45] A. W. Labrador, 2011, ICRC, 6, 55
[46] W. Menn, 2011, ICRC, 6, 35
[47] V. Formato, 2011, ICRC, 6, 75
[48] W. Gillard, 2011, ICRC, 6, 173
[49] T. Kobayashi, et al., 2004, ApJ, 601, 340
[50] G. Sinnis, 2009, ICRC (OG1 Rapporteur talk)
[51] D. Grasso, et al., 2009, Astropart. Phys., 32, 140
[52] D. Grasso, et al., 2011, Nucl. Instr. Meth. Phys. Res. A, 630, 48
[53] J. Chang, et al., 2008, Nature, 456, 362
[54] A. Moiseev, 2011, ICRC, 6, 151
[55] M. Ackermann, et al., 2010, Phys. Rev. D, 82, 092004
[56] A. A. Abdo, et al., 2009, Phys. Rev. Lett., 102, 181101
[57] F. Aharonian, et al., 2009, A&A, 508, 561
[58] E. Mocchiutti, 2011, ICRC, 6, 63
[59] O. Adriani, et al., 2011, Phys. Rev. Lett., 106, 201101

[60] P. Picozza, 2011, ICRC (highlight), in press
[61] D. B. Tridon, 2011, ICRC, 6, 43
[62] T. Kobayashi, 2011, ICRC, 6, 59
[63] M. Pato, M. Lattanzi and G. Bertone, 2010, JCAP, 12, 20
[64] N. Volkov, 2011, ICRC, 6, 261
[65] A. Panov and V. I. Zatsepin, 2011, ICRC, 6, 13
[66] L. G. Sveshnikova, 2011, ICRC, 6, 184
[67] Y. Guo, 2011, ICRC, 6, 265
[68] E. Orlando, 2011, ICRC, 6, 269
[69] O. Adriani, et al., 2009, Nature, 458, 607
[70] O. Adriani, et al., 2010, Astropart. Phys., 34, 1
[71] L. Rossetto, 2011, ICRC, 6, 31
[72] S. W. Barwick, et al., 1997, Nucl. Instr. Meth. Phys. Res. A, 400, 34
[73] J. Vandenbroucke, 2011, ICRC, 9, 161
[74] R. R. Daniel and S. A. Stephens, 1965, Phys. Rev. Lett., 15, 769
[75] D. Mueller and K.-K. Tang, 1987, ApJ, 312, 183
[76] P. Colin, 2011, ICRC, 6, 189
[77] M. Urban, et al., 1990, Nucl. Phys. B Proc. Suppl., 14, 223
[78] G. Di Sciascio, 2011, ICRC, 1, 30
[79] O. Adriani, et al., 2010, Phys. Rev. Lett., 105, 121101
[80] K. Sakai, 2011, ICRC, 6, 106
[81] A. Bruno, 2011, ICRC, 6, 82
[82] A. Turundaewskiy, 2011, ICRC, 6, 340
[83] O. Martinez Bravo, 2011, ICRC, 6, 400
[84] V. W. Jones, 2011, ICRC, 6, 328
[85] S. Torii, 2011, ICRC, 6, 344
[86] K. Yoshida, 2011, ICRC, 6, 360
[87] S. Ozawa, 2011, ICRC, 6, 67
[88] S. Torii, et al., 2002, Nucl. Phys. B Proc. Suppl., 113, 103
[89] J. Chang, 2011, ICRC, #377
[90] C. Feng, 2011, ICRC, 6, 2
[91] J. W. Mitchell, 2011, ICRC, 6, 98
[92] A. Kounine, 2011, ICRC (highlight), in press
[93] V. Bindi, 2010, Nucl. Instr. Meth. Phys. Res. A, 617, 462
[94] K. Lübelsmeyer, et al., 2011, Nucl. Instr. Meth. Phys. Res. A, 654, 639
[95] P. Zuccon, 2009, ICRC, Lodz, Poland